

Tree tensor network state approach for solving hierarchical equations of motion

Yaling Ke^{1, a)}

Institute of Physics, University of Freiburg, Hermann-Herder-Strasse 3, 79104 Freiburg, Germany

The hierarchical equations of motion (HEOM) method is a numerically exact open quantum system dynamics approach. The method is rooted in an exponential expansion of the bath correlation function, which in essence strategically reshapes a continuous environment into a set of effective bath modes that allow for more efficient cutoff at finite temperatures. Based on this understanding, one can map the HEOM method into a Schrödinger-like equation, with a non-Hermitian super Hamiltonian for an extended wave function being the tensor product of the central system wave function and the Fock state of these effective bath modes. In this work, we explore the possibility of representing the extended wave function as a tree tensor network state (TTNS), the super Hamiltonian as a tree tensor network operator of the same structure as the TTNS, as well as the application of a time propagation algorithm using the time-dependent variational principle. Our benchmark calculations based on the spin-boson model with a slow-relaxing bath show that the proposed HEOM+TTNS approach yields consistent results with that of the conventional HEOM method, while the computation is considerably sped up. Besides, the simulation with a genuine TTNS is four times faster than a one-dimensional matrix product state decomposition scheme.

The efficient simulation of open quantum system dynamics lies at the heart of a great variety of chemical and physical applications,¹⁻³ ranging from efficient energy and charge transfer in natural and artificial photosynthetic systems to quantum transport in nanoscale electronic devices.⁴⁻⁷ Over the past few decades, the hierarchical equations of motion (HEOM) method has grown into a mainstream non-perturbative and non-Markovian open quantum system dynamics approach.⁸⁻¹⁶ The core idea of the method is based on an exponential series expansion of the bath correlation function as well as successively taking time-derivative of the reduced system density operator in the influence functional formalism, so as to construct a group of auxiliary density operators (ADOs) that obey a hierarchical set of differential equations.

While the HEOM method has gained tremendous success aided by abundant optimization schemes and advances in computational architecture,¹⁷⁻²⁵ its applications hit a hard wall in the cases where the central system size is large, many exponential terms (or effective bath modes) are required to reproduce the original bath correlation function, and a deep hierarchical depth is necessitated to account for the strong system-bath coupling accurately. This is because the computational cost grows exponentially with the increase of these factors. Recently, these limitations have been effectively broached by employing the matrix product states (MPS),²⁶ also known as tensor trains (TT) decomposition²⁷ of these ADOs.²⁸⁻³¹ MPS/TT provides a compact and ideal way to encode one-dimensional (1D) short-range quantum many-body system correlation,³² by representing the multi-dimensional wave function as the product of a chain of low-rank tensors. When the entanglements are well

confined within the near neighboring tensors over a long time, the computational cost of the HEOM+MPS/TT method scales linearly with the system size, the number of effective bath modes, and the hierarchical depth. However, it is not often the case for the HEOM+MPS/TT method, because in addition to the strong correlation among system degrees of freedom (DoF), the system DoF may also be strongly coupled to every effective bath mode. As a consequence, the correlation would quickly spread over a long distance along the MPS chain, and very large bond dimensions are needed to obtain accurate results. Therefore, it is important to go beyond the MPS/TT ansatz and explore the combination of the HEOM method with other higher-dimensional tensor network state structures that can more efficiently encode the inherent entanglement between the system DoFs and effective bath modes.

In this work, we will demonstrate the applicability of tree tensor network state (TTNS) which is a generalization of the MPS/TT into a tree-shaped network of tensors,³³⁻⁴⁵ and a time propagation algorithm based on the time-dependent variational principle (TDVP)⁴⁶⁻⁴⁸ for solving the HEOM method.

In general, an open quantum system describes a central system of interest coupled to a macroscopic environment, and the Hamiltonian reads

$$H = H_S + H_B + H_{SB}, \quad (1)$$

where H_S , H_B , and H_{SB} correspond to the system, bath Hamiltonian, and their interaction, respectively. As a demonstration of the concept, we start by considering a simple but paradigmatic open quantum system, the spin-boson model, where the system Hamiltonian is given by

$$H_S = \epsilon\sigma_z + \Delta\sigma_x. \quad (2)$$

Here, the energy bias between two spin states is given by 2ϵ and Δ denotes the coupling between two states.

^{a)}Electronic mail: yaling.ke@physik.uni-freiburg.de

The spin is coupled to a dissipative bosonic environment, modeled as a phonon bath comprised of an infinite number of harmonic oscillators,

$$H_B = \sum_j \left(\frac{p_j^2}{2} + \frac{1}{2} \omega_j^2 q_j^2 \right), \quad (3)$$

where q_j and p_j are the mass-weighted position and conjugated momentum operator of the j th harmonic oscillator, and ω_j is the corresponding frequency. The system-bath coupling Hamiltonian H_{SB} takes a linear form with respect to the bath coordinate q_j ,

$$H_{SB} = \sigma_z \sum_j c_j q_j, \quad (4)$$

and the system-bath coupling operator in the system subspace is given by σ_z , the coupling strength specified by c_j .

The composite system-bath dynamics are described by the density operator $\rho(t)$. Note that, we assume the system and bath are factorized at the initial moment and the bath is in its own thermal equilibrium state at inverse temperature β . Then, the initial density operator $\rho(0)$ is given by

$$\rho(0) = \rho_S(0) \otimes \frac{e^{-\beta H_B}}{\text{Tr}_B \{ e^{-\beta H_B} \}}. \quad (5)$$

In this case, in the reduced system dynamics $\rho_S(t) = \text{tr}_B \{ \rho(t) \}$ where all environmental DoFs are traced out, the influence of the environment on the system is characterized statistically in a time correlation function

$$C(t) = \frac{1}{\pi} \int_{-\infty}^{\infty} \frac{e^{-i\omega t}}{1 - e^{-\beta\omega}} J(\omega) d\omega. \quad (6)$$

The spectral density function $J(\omega)$ encodes the coupling-weighted density of states of the bath in frequency space, defined by

$$J(\omega) = \frac{\pi}{2} \sum_j \frac{c_j^2}{\omega_j} \delta(\omega - \omega_j). \quad (7)$$

For some specific forms of $J(\omega)$, such as Drude-Lorentz spectral density function,

$$J(\omega) = 2\lambda \frac{\omega\Omega}{\omega^2 + \Omega^2}, \quad (8)$$

where Ω is the bath characteristic frequency and λ quantifies the system-bath coupling strength, the bath correlation function in Eq.(6) can be expanded analytically into an exponential summation,

$$C(t) = \sum_{p=0}^{\infty} \lambda \eta_p e^{-i\gamma_p t}. \quad (9)$$

The explicit expressions of η_p and γ_p depend on the sum-over-pole decomposition scheme of the Bose distribution function $f(\omega) = 1/(1 - e^{-\beta\omega})$. Throughout this

work, we adopt the Padé pole decomposition scheme^{19,49} and the explicit expressions for η_p and γ_p can be found in the supporting information (SI). At finite temperatures, the infinite summation in Eq.(9) can be cut off at a finite P , which is chosen large enough to well reproduce the original bath correlation function. For an arbitrary form of the spectral density function, the exponential expansion analogous to Eq.(9) can be implemented numerically.^{23,24,50}

In fact, the exponential expansion in Eq.(9) lays the groundwork for the derivations of the HEOM method. For a detailed derivation of the method, we refer readers to a review Ref. 16 and the references therein. Here, we only briefly introduce the main concept of the method. The key is to introduce a group of ADOs, $\rho^{\mathbf{n}}(t)$, where the superscript $\mathbf{n} = (n_0, \dots, n_p, \dots, n_P)$ is an ordered set of $P + 1$ non-negative integers and each n_p is associated with a frequency component γ_p in Eq.(9). These ADOs are closed with respect to the time-derivative operation, which yields

$$\begin{aligned} i \frac{d\rho^{\mathbf{n}}(t)}{dt} = & H_S \rho^{\mathbf{n}}(t) - \rho^{\mathbf{n}}(t) H_S - i \sum_{p=0}^P n_p \gamma_p \rho^{\mathbf{n}}(t) \\ & + \sum_{p=0}^P \sqrt{\lambda(n_p + 1)} \left(\sigma_z \rho^{\mathbf{n}_p^+}(t) - \rho^{\mathbf{n}_p^+}(t) \sigma_z \right) \\ & + \sum_{p=0}^P \sqrt{\lambda n_p} \left(\eta_p \sigma_z \rho^{\mathbf{n}_p^-}(t) - \eta_p^* \rho^{\mathbf{n}_p^-}(t) \sigma_z \right), \end{aligned} \quad (10)$$

where $\mathbf{n}_p^{\pm} = (n_0, \dots, n_p \pm 1, \dots, n_P)$. Directly propagating Eq.(10) with a certain hierarchy truncation scheme is termed as the conventional HEOM method. The simplest truncation scheme is to set $\rho^{\mathbf{n}}(t) = 0$ when $\sum_p n_p > L$ and L is the hierarchical truncation tier. Using this truncation scheme, the number of elements to be stored and propagated is $\frac{(P+1+L)!}{(P+1)!L!} d^{2N_s}$, where N_s is the number of system DoFs and d is the size of basis set per system DoF (for the spin-boson model, we have $N_s = 1$ and $d = 2$). As such, the conventional HEOM method is formidably expensive in the cases of many bath poles, a deep truncation tier, and a large central system. An alternative way to reduce the computational cost and memory requirement is to employ tensor network states. To this end, it is opportune to reformulate the above hierarchical set of differential equations into a Schrödinger-like equation,^{29,31}

$$i \frac{d|\Psi(t)\rangle}{dt} = \mathcal{H}|\Psi(t)\rangle, \quad (11)$$

via the introduction of an effective phonon bath and the density matrix purification scheme.⁵¹⁻⁵⁶

First, $|n_p\rangle$ can be interpreted as the basis in the occupation number representation of a virtual dissipative harmonic oscillator. A pair of creation and annihilation operators, b_p^\dagger and b_p are introduced, and they act on $|n_p\rangle$

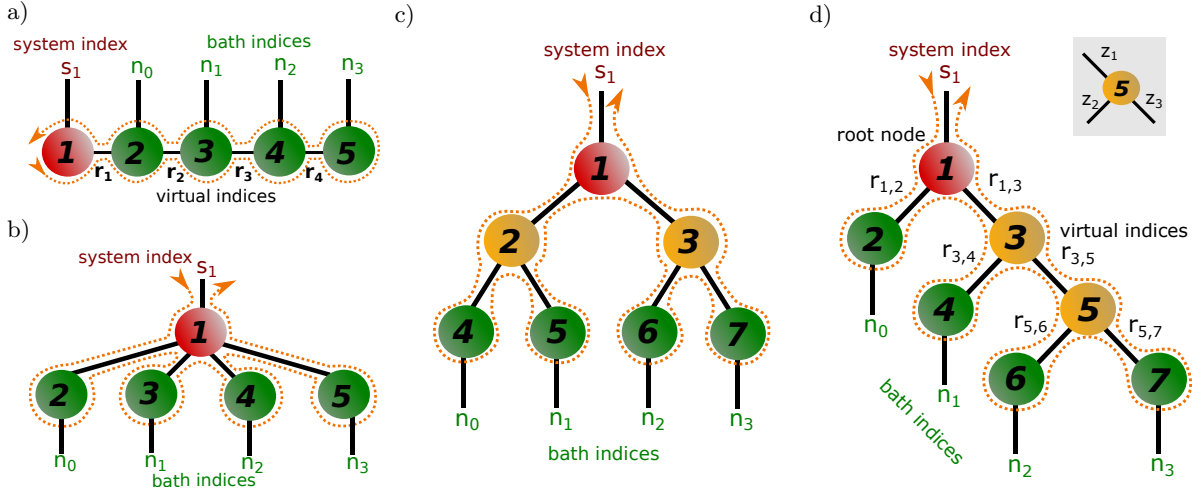


FIG. 1. Examples of the MPS/TT (a) and three TTNS decompositions (b, c, and d) in the graphical notation of the extended wave function $|\Psi(t)\rangle$ (see Eq. (14)) with $P = 3$ for the spin-boson model. The circle nodes represent the tensors, black dangling lines denote the physical indices, and shared links correspond to virtual indices. The orange dotted lines with arrows specify the ordered sequence sweeping through all nodes in the entire TTNS, which start and end at the root node.

to yield

$$b_p^\dagger |n_p\rangle = \sqrt{n_p + 1} |n_p + 1\rangle, \quad (12a)$$

$$b_p |n_p\rangle = \sqrt{n_p} |n_p - 1\rangle. \quad (12b)$$

All these virtual modes constitute an effective phonon bath, which encrypts the statistical information of the original bath as well as its influence on the system dynamics (see Eqs. (3) and (4)). When all these effective modes are placed in their ground states, i.e., for the particular configuration of the Fock state $|\mathbf{n}\rangle = |0, \dots, 0\rangle$, the reduced system density operator is reproduced, $\rho_S(t) = \rho^{(0, \dots, 0)}(t)$. Certain bath-related properties can be extracted from the higher-order ADOs.^{13,57–59}

Second, each ADO is usually expressed as a density matrix in the Hilbert space, but it can also be recast into a rank- N_s tensor,

$$|\rho^n(t)\rangle\rangle \equiv \sum_{s_1 \dots s_{N_s}} C_{s_1 \dots s_{N_s}}^n(t) |s_1 \dots s_{N_s}\rangle. \quad (13)$$

where s_i ranges from 1 to d^2 . For more theoretical and technical details with regard to this space transformation, we refer readers to Refs. 51–56.

All the ADOs combined comprise an extended wave function in the enlarged space

$$|\Psi(t)\rangle = \sum_{\substack{s_1 \dots s_{N_s} \\ n_0 \dots n_P}} C_s^n(t) |s_1 \dots s_{N_s}\rangle \otimes |n_0 \dots n_P\rangle. \quad (14)$$

The reduced system density operator is obtained by the partial product $|\rho_S(t)\rangle\rangle \equiv \langle \mathbf{n} = \mathbf{0} | \Psi(t)\rangle$. A system observable $\langle O(t) \rangle$ is obtained by

$$\langle O(t) \rangle = \text{tr}_S \{ O \rho_S(t) \} = \langle \mathbf{n} = \mathbf{0} | \bigotimes_{i=1}^{N_s} \langle \mathbb{1}_d^i | \hat{O} | \Psi(t) \rangle, \quad (15)$$

where O can be any operator in the system subspace, and $\hat{O} = O \otimes \mathbb{1}_d$ with $\mathbb{1}_d$ being an $d \times d$ unit matrix. $\mathbb{1}_d$ is a vector of length d^2 , obtained by vectorizing $\mathbb{1}_d$. For instance, $\mathbb{1}_2 = (1 \ 0 \ 0 \ 1)^{\text{transpose}}$.

The super Hamiltonian \mathcal{H} in Eq. (11) can be written out explicitly with the operators introduced in Eq. (12) as

$$\begin{aligned} \mathcal{H} = & \mathcal{H}_S - i \sum_{p=0}^P \gamma_p b_p^\dagger b_p + \sqrt{\lambda} \hat{\sigma}_z \sum_{p=0}^P (b_p + \eta_p b_p^\dagger) \\ & - \sqrt{\lambda} \tilde{\sigma}_z \sum_{p=0}^P (b_p + \eta_p^* b_p^\dagger), \end{aligned} \quad (16)$$

where $\mathcal{H}_S = \epsilon (\hat{\sigma}_z - \tilde{\sigma}_z) + \Delta (\hat{\sigma}_x - \tilde{\sigma}_x)$ with $\hat{\sigma}_{z/x} = \sigma_{z/x} \otimes \mathbb{1}_2$, $\tilde{\sigma}_{z/x} = \mathbb{1}_2 \otimes \sigma_{z/x}$, and $\mathbb{1}_2$ being a 2×2 unit matrix. The super operator \mathcal{H}_S originates from the space transformation of H_S in correspondence with Eq. (13). It is worth noting that the super Hamiltonian \mathcal{H} is non-Hermitian. As such, the norm of the extended wave function $|\Psi(t)\rangle$ is not conserved.

The direct time integration of Eq. (11) along with the explicit definition of the extended wave function $|\Psi(t)\rangle$ and super Hamiltonian \mathcal{H} given in Eq. (14) and Eq. (16), respectively, is usually an intractable task as the size of the coefficient tensor $C_s^n(t)$ scales exponentially with the number of extended system DoFs, $N = N_s + P + 1$. This huge amount of data can be compressed in the format of a tensor network state, which is a structured product of low-rank tensors.

The well-established MPS/TT format is a special and widely-used instance of tensor network states, where the tensors are arranged into a one-dimensional chain.^{26,27,60–62} The high-rank coefficient tensor $C_s^n(t)$ in the extended wave function $|\Psi(t)\rangle$ can be approximated

in the MPS/TT formalism as

$$\begin{aligned} C_s^n(t) &\approx \sum_{r_1 \cdots r_{N-1}} A_{r_1, s_1}^{[1]} \cdots A_{r_{N_s}, r_{N_s+1}, n_0}^{[N_s+1]} \cdots A_{r_{N-1}, n_P}^{[N]} \\ &\approx \text{Contr} \{ A_{s_1}^{[1]} \cdots A_{n_0}^{[N_s+1]} \cdots A_{n_P}^{[N]} \}. \end{aligned} \quad (17)$$

Here, $A^{[i]}$ are rank-3 tensors with one physical index (s_i or n_p) and two virtual indices r_{i-1} and r_i , except for $A^{[1]}$ and $A^{[N]}$, which are rank-2 tensors and thus have only one virtual index. The virtual index r_i runs from 1 to D_i , where the bond dimension D_i is a controllable parameter, that can be systematically increased to reduce the degree of approximation in Eq. (17). The maximum value among $\{D_i\}$ is designated as the maximal bond dimension D_{\max} . An example of the MPS/TT representation of $|\Psi(t)\rangle$ with $P = 3$ is illustrated graphically in Fig. 1 (a). The circle nodes correspond to the tensors. The dangling legs denote the physical indices, and the connected link between two neighboring nodes is assigned with a virtual index r_i . The summation over a virtual index shared between two tensors is called the contraction. Contracting all virtual indices (denoted in Eq. (17) as Contr) reproduces approximately $C_s^n(t)$.

The TTNS is an extension of the MPS/TT beyond 1D geometry and thus can accommodate a more complicated entanglement network.^{33–45} It is also called hierarchical Tucker format,⁶³ which is the ansatz behind an important quantum dynamics approach, multi configuration time-dependent Hartree and its multi-layer variant.^{64–69} A general TTNS connects all tensors into a tree structure and the network is loop-free,⁷⁰ which means that there exists a unique path between any two tensors. A TTNS representation for $C_s^n(t)$ in the extended wave function $|\Psi(t)\rangle$ is directly analogous to Eq. (17),

$$C_s^n(t) \approx \text{Contr} \{ T_{s_1}^{[1]} T_{n_0}^{[2]} T_X^{[3]} \cdots T^{[k]} \cdots T_{n_P}^{[K]} \}, \quad (18)$$

except that $T^{[k]}$ is now a rank- z tensor, where z can be higher than 3.

There are many different ways to connect the tensors into a tree-shaped network. For example, we show in Fig. 1 the graphical representation of several different TTNS decompositions for the extended wave function $|\Psi(t)\rangle$ with $P = 3$. A circle node with z legs corresponds to a rank- z tensor. For convenience, the nodes are enumerated and we take the TTNS in Fig. 1 (d) as an example to introduce the notations that will be used in what follows. Similar to an MPS/TT, there are nodes assigned with one dangling leg denoting the physical index s_1/n_p , such as nodes $T_{s_1}^{[1]}$, $T_{n_0}^{[2]}$, $T_{n_1}^{[4]}$, $T_{n_2}^{[6]}$, and $T_{n_3}^{[7]}$. Here, we assign the nodes with the dangling leg corresponding to the system indices and bath indices as the system nodes (red-shaded) and bath nodes (green-shaded), respectively. A TTNS can also have connecting nodes, which have exclusively connected legs, i.e., virtual indices, like nodes $T_X^{[3]}$ and $T_X^{[5]}$. Therefore, the number of nodes K can be larger than N . Every node can have none or multiple children nodes. For example, the first node $T^{[1]}$ has

two children nodes, $T^{[2]}$ and $T^{[3]}$. $T^{[2]}$ has no children node. Leaves are the nodes without children nodes. The first system node is denoted as the root node, as shown in Fig. 1 (d). The root node has no parent node. Other than the root node, every node has a parent node, which is the adjacent node on the path pointing toward the root node. For each node, all the legs are enumerated in a counter-clockwise manner with the bond connected to the parent node designated as the first leg, and the dangling leg (if it has) as the last leg, as shown exemplarily for node $T^{[5]}$ at the top-right corner of Fig. 1 (d).

Ideally, strongly entangled tensors should be arranged as closely as possible. The tree shape in Fig. 1 (b) is in alignment with the entanglement topology of the super Hamiltonian \mathcal{H} in Eq. (16) where all effective bath modes are directly coupled to the system DoF and they are independent of each other. However, the tensor network contraction cost for this tree structure scales as $\mathcal{O}(D_{\max}^{P+1})$, which can be very expensive or even intractable when many effective environmental modes are taken into account. This issue can be resolved by inserting connecting nodes (yellow-shaded) between the system node and bath nodes, as illustrated in Fig. 1 (c) and (d). In the cases where every environmental mode imposes the same effect on the system dynamics, a balanced tree structure as in Fig. 1 (c) can be chosen, such that the distances between each bath node and the system node are equal. Otherwise, a more unbalanced tree structure can be adopted when the influence of some effective virtual phonon modes on the system dynamics is much stronger than the others. It is likely, that the impact of the effective phonon modes with a large Padé pole number p on the system dynamics is smaller than those with a smaller p . Thereby, in this work, we adopt the unbalanced TTNS in Fig. 1 (d) in our simulations.

Recently, by taking advantage of the special structure of the HEOM method, Yan and Shi⁷¹ proposed an efficient split operator method for propagating the binary TTNS. The method is implemented by successively constructing and updating the local MPS chain on the path connecting the system node and a bath tensor. In this work, we present an alternative route that directly employs the TDVP time propagation scheme on the whole TTNS.

To this end, the super Hamiltonian \mathcal{H} in Eq. (16) needs to be decomposed into the product of tree tensor network operators (TTNO), which have the same network structure as the TTNS,

$$\mathcal{H} = \text{Contr} \left\{ W_{s_1, s'_1}^{[1]} W_{n_0, n'_0}^{[2]} \left(\prod_{p=1}^{P-1} W_X^{[2p+1]} W_{n_p, n'_p}^{[2p+2]} \right) W_{n_P, n'_P}^{[2P+1]} \right\}, \quad (19)$$

as exhibited graphically in Fig. 2 (a) for $P = 3$. The

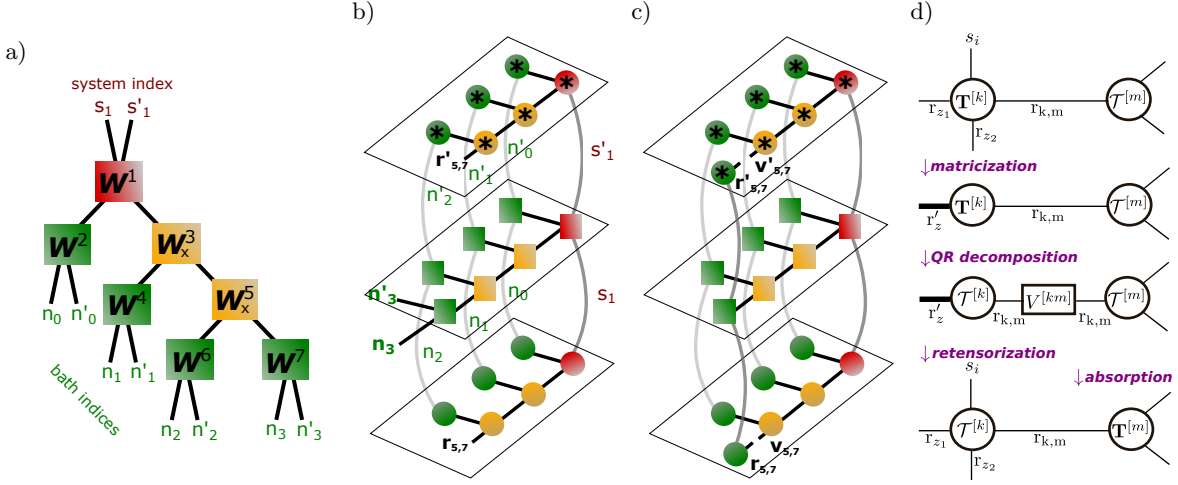


FIG. 2. (a) An example of the TTNO decomposition of the super Hamiltonian \mathcal{H} (see Eq. (16)), which has the same network structure as the TTNS in Fig. 1 (b). To distinguish the TTNO from the TTNS in the graphical notation, each tensor in the TTNO is represented as a rectangle node. (b) and (c) display an example of the effective Hamiltonian $H_{[k]}^{\text{eff}}$ (see Eq. (26)) for node $T^{[7]}$ and $G_{[km]}^{\text{eff}}$ (see Eq. (27)) for the link between nodes $T^{[5]}$ and $T^{[7]}$, respectively. The nodes with an asterisk denote taking their complex conjugation. (d) Schematic illustration of the tensor operations.

TTNO tensors $W_{s_1, s'_1}^{[1]}$ and $W_{n_p, n'_p}^{[2p+2]}$ in Eq. (19) read

$$W_{s_1, s'_1}^{[1]} = \begin{pmatrix} \mathcal{H}_S & \hat{\sigma}_z & -\tilde{\sigma}_z & \mathbb{1}_4 \\ \hat{\sigma}_z & & & \\ -\tilde{\sigma}_z & & & \\ \mathbb{1}_4 & & & \end{pmatrix}, \quad (20)$$

$$W_{n_p, n'_p}^{[2p+2]} = \begin{pmatrix} \mathbb{1}_L & & & \\ \sqrt{\lambda} (b_p + \eta_p b_p^\dagger) & & & \\ \sqrt{\lambda} (b_p + \eta_p^* b_p^\dagger) & & & \\ -i\gamma_p b_p^\dagger b_p & & & \end{pmatrix}, \quad (21)$$

where the terms equal to zero have been left blank in Eq. (20). $\mathbb{1}_L$ is an $L \times L$ unit matrix. W_X is a rank-3 connecting tensor of size $4 \times 4 \times 4$ with the entries

$$W_X[i, j, k] = \frac{\delta_{ij}\delta_{k=1} + \delta_{ik}\delta_{j=1}}{2\delta_{i=1} + \delta_{i \neq 1}}. \quad (22)$$

With the TTNS and TTNO expression for the extended wave function $|\Psi(t)\rangle$ and the super Hamiltonian \mathcal{H} explicitly given in Eqs. (18) and (19), respectively, we can use the TDVP-based time propagation algorithm to solve Eq. (11). TDVP algorithm has been proven to be a stable and efficient time propagation scheme for the MPS/TT. ^{72–78} The feasibility of the TDVP algorithm on the TTNS, the detailed derivation and related numerical analyses have been reported in Refs. 46–48. Here, we only concisely discuss the implementation of the algorithm for our model and provide a pseudocode.

In the one-site version of the TDVP algorithm, the Schrödinger equation in Eq. (11) is solved by projecting the wave function into the so-called tangent space, i.e., a manifold of all TTNSs with fixed bond dimensions, ^{46–48}

$$i \frac{|\Psi[T]\rangle}{\partial t} = \mathcal{P}_{\mathcal{M}\{\Psi[T]\}} \mathcal{H} |\Psi[T]\rangle. \quad (23)$$

The explicit expression of the tangent space projection operator $\mathcal{P}_{\mathcal{M}\{\Psi[T]\}}$ can be found in Refs. 46–48. By using Trotter breakups, the projected time-dependent Schrödinger equation in Eq. (23) can be integrated locally, where each tensor $T^{[k]}$ and the link $V^{[km]}$ between node k and one of its neighboring node m in a specified sequence are updated according to the following equations

$$\frac{\partial T^{[k]}(t)}{\partial t} = -i H_{[k]}^{\text{eff}} T^{[k]}(t), \quad (24)$$

$$\frac{\partial V^{[km]}(t)}{\partial t} = i G_{[km]}^{\text{eff}} V^{[km]}(t), \quad (25)$$

while all other tensors are fixed. The effective local Hamiltonian $H_{[k]}^{\text{eff}}$ in Eq. (24) and $G_{[km]}^{\text{eff}}$ in Eq. (25) are given by

$$H_{[k]}^{\text{eff}} = \text{Contr}'_k \left\{ T_{s_1}^{[1]} W_{s_1, s'_1}^{[1]} T_{s'_1}^{[1]*} \dots T^{[k-1]} W^{[k-1]} T^{[k-1]*} W^{[k]} T^{[k+1]} W^{[k+1]} T^{[k+1]*} \dots T^{[K]} W_{n_P, n'_P}^{[K]} T_{n'_P}^{[K]*} \right\}, \quad (26)$$

$$G_{[km]}^{\text{eff}} = \text{Contr}''_{km} \left\{ T_{s_1}^{[1]} W_{s_1, s'_1}^{[1]} T_{s'_1}^{[1]*} \dots T^{[k]} W^{[k]} T^{[k]*} \dots T_{n_P}^{[K]} W_{n_P, n'_P}^{[K]} T_{n'_P}^{[K]*} \right\}. \quad (27)$$

Here, we use the Einstein convention that the duplicate indices are summed over. The asterisk denotes taking the complex conjugation of the tensor. Contr'_k denotes contracting over all physical and virtual indices in the TTNS decomposition of $C_s^n(t)$ and $C_s^{n*}(t)$ as well as the

TTNO expression for \mathcal{H} , except for leaving the indices connected to $T^{[k]}$ and $T^{[k]*}$ and physical indices to $W^{[k]}$ open. For $\text{Contr}''_{[km]}$, the bond connecting $T^{[k]}$ and $T^{[m]}$ as well as the bond connecting $T^{[k]*}$ and $T^{[m]*}$ are left open. As an example, we show the graphical representation of $H_{[7]}^{\text{eff}}$ and $G_{[57]}^{\text{eff}}$ in Fig. 2 (b) and (c), respectively.

A full TDVP step starts from a canonicalized TTNS, where all tensors except for the root node are orthonormalized, $\mathcal{T}^{[1]}(t), \mathcal{T}^{[2]}(t), \dots, \mathcal{T}^{[K]}(t)$, and is accomplished when all tensors are propagated to $\mathcal{T}^{[1]}(t + \Delta t), \mathcal{T}^{[2]}(t + \Delta t), \dots, \mathcal{T}^{[K]}(t + \Delta t)$ after a sweeping along the entire network, as illustrated by the orange dotted lines in Fig. 1. A full sweeping procedure starts and ends at the root node, and every node is entered and exited $n_c^k + 1$ times where n_c^k is the number of the children nodes to node k . For example, a sweep over the TTNS in Fig. 1 (d) goes through the nodes sequentially, and the path is $1 \rightarrow 2 \rightarrow 1 \rightarrow 3 \rightarrow 4 \rightarrow 3 \rightarrow 5 \rightarrow 6 \rightarrow 5 \rightarrow 7 \rightarrow 5 \rightarrow 3 \rightarrow 1$. To keep track of the time evolution, we introduce a variable h_k and it is initialized as $h_k = 0$ before the sweeping procedure starts. Moving from node k to a neighboring node m along the direction of the sweeping path, the following steps are implemented:

1. Evolve $\mathbf{T}^{[k]}(t + h_k)$ forward in time according to

$$\mathbf{T}^{[k]} \left(t + h_k + \frac{\Delta t}{n_c^k + 1} \right) = e^{-iH_{[k]}^{\text{eff}} \frac{\Delta t}{n_c^k + 1}} \mathbf{T}^{[k]}(t + h_k), \quad (28)$$

and then update $h_k = h_k + \frac{\Delta t}{n_c^k + 1}$. $H_{[k]}^{\text{eff}}$ is computed with $\mathcal{T}^{[1]}(t + h_1), \dots, \mathcal{T}^{[k-1]}(t + h_{k-1}), \mathcal{T}^{[k+1]}(t + h_{k+1}), \dots, \mathcal{T}^{[K]}(t + h_K)$.

2. Permute the indices of $\mathbf{T}^{[k]}(t + h_k)$ and then reshape the tensor into a matrix such that the index $r_{k,m}$ corresponding to the bond connecting nodes k and m now serves as the column of the matrix, while all other indices are grouped into one index as the row of the matrix; Conduct the QR decomposition of the matricized $\mathbf{T}^{[k]}(t + h_k)$ into $\mathcal{T}^{[k]}(t + h_k)$ and $V^{[km]}(t + h_k)$; Retensorize $\mathcal{T}^{[k]}(t + h_k)$ as a new local tensor on node k .

3. Evolve $V^{[km]}(t + h_k)$ in time according to

$$V^{[km]}(t + h_m) = e^{iG_{[km]}^{\text{eff}}(h_k - h_m)} V^{[km]}(t + h_k), \quad (29)$$

where $G_{[km]}^{\text{eff}}$ is computed with $\mathcal{T}^{[1]}(t + h_1), \dots, \mathcal{T}^{[k]}(t + h_k), \dots, \mathcal{T}^{[K]}(t + h_K)$.

4. Absorb $V^{[km]}(t + h_m)$ into $\mathcal{T}^{[m]}(t + h_m)$ to obtain $\mathbf{T}^{[m]}(t + h_m)$.

The tensor operations in the second and fourth steps are schematically illustrated in Fig. 2 (d). After implementing the above steps, the orthogonality center in the TTNS is also moved from node k to the adjacent node m .

To assess the accuracy and performance of the proposed HEOM+TTNS method against the conventional HEOM method, we first conduct a benchmark calculation on the spin-boson model. The spin is initially placed in the spin-up state. The parameters can be found in the caption of Fig. 3. Note that, we adopt a much smaller value for Ω than other parameters, which indicates that the bath relaxation is slow as compared to other system dynamical processes, and the non-Markovian feature in this case can be strong. We inspected the spin dynamics $\langle \sigma_z(t) \rangle = \text{tr}\{\sigma_z \rho(t)\}$ and found that the converged result using the conventional HEOM method is obtained with a very deep truncation tier $L = \sum_{p=0}^P n_p = 50$ and $P = 3$. Using the HEOM+TTNS method with the TTNS displayed in Fig. 1 (d), $\langle \sigma_z(t) \rangle$ is calculated by

$$\langle \sigma_z(t) \rangle = \text{Contr} \left\{ \mathbb{1}_2[s_1] \hat{\sigma}_z[s_1, s'_1] \mathbf{T}_{s'_1}^{[1]} \mathcal{T}_{n_0=0}^{[2]} \left(\prod_{p=1}^{P-1} \mathcal{T}_X^{[2p+1]} \mathcal{T}_{n_p=0}^{[2p+2]} \right) \mathcal{T}_{n_P=0}^{[2P+1]} \right\}, \quad (30)$$

which is graphically illustrated in Fig. 3 (a). For every effective bath mode, we take $0 \leq n_p \leq L$, which means that actually more ADOs are taken into account than in the conventional HEOM method. We found that with a very low maximal bond dimension $D_{max} = 5$, the result obtained through the HEOM+TTNS method is already in excellent agreement with that obtained through the conventional HEOM method, as shown in Fig. 3 (b).

For a fair comparison, all the codes are written using Julia programming language and our simulations are run on a single CPU core of an Apple MacBook Pro laptop with M1 chip. For the conventional HEOM method, we use an exponential integrator as proposed in Ref. 79, which requires less memory usage as compared to Runge-Kutta methods. Every simulation step takes on average 6.7 seconds with a time step $\Delta t = 0.025$ fs and requires a memory of 7.6 GB. Using the HEOM+TTNS method with the previously stated TDVP integration scheme, we gain a significant speed-up in computational time and save in memory usage. Every simulation step takes only 0.028 seconds in CPU time and memory usage of 10 MB. Besides, it is also found that the maximally allowed time step in the HEOM+TTNS method is $\Delta t = 0.5$ fs, much larger than that used in the conventional HEOM method. We should mention that our code for the conventional HEOM method is not fully optimized. The introduction of the filtering algorithm proposed by Shi *et al.*¹⁸ would greatly improve its efficiency. However, the simulation time using the HEOM+TTNS method grows nearly linearly with the increase of pole number P and truncation tier L , in contrast to the factorial scaling in the conventional HEOM method. As such, even for the relatively simple spin-boson model, we found that the simulation using the HEOM+TTNS method is generally much faster than the conventional HEOM method.

We also tested the MPS/TT decomposition of the extended wave function $|\Psi(t)\rangle$ for the above model (see

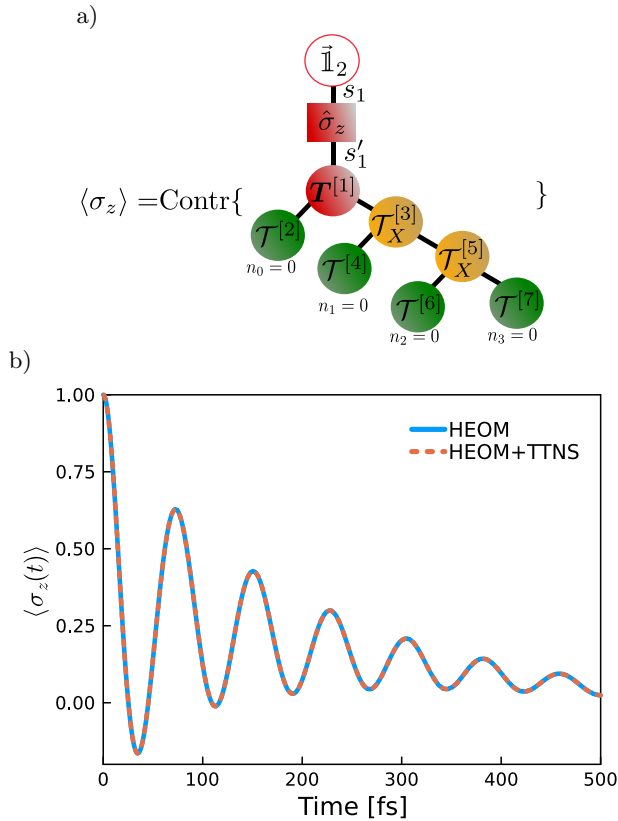


FIG. 3. (a) Graphical illustration of calculating $\langle \sigma_z(t) \rangle$ (see Eq. (30)) with the TTNS shown in Fig. 1 (d). (b) Dynamics of the spin-boson model calculated using the conventional HEOM with a hierarchical truncation tier $L = 50$ and the HEOM+TTNS method with a maximal bond dimension $D_{max} = 5$. The following parameters are used: $\epsilon = 50 \text{ cm}^{-1}$, $\Delta = 200 \text{ cm}^{-1}$, $\beta^{-1} = 300K$, $\lambda = 100 \text{ cm}^{-1}$, and $\Omega = 10 \text{ cm}^{-1}$.

the tensor network structure in Fig. 1 (a)) and the matrix product operator format of the super Hamiltonian \mathcal{H} is obtained using ITensor Package.⁸⁰ The same time propagation algorithm and code as in the HEOM+TTNS method are used. For this model, although we found that the result of the HEOM+MPS/TT method (data not shown) also converges with a maximal bond dimension of $D_{max} = 5$, every simulation step is four times slower than that of the HEOM+TTNS method. This implies the pure influence of a tree shape in determining the practical computational cost.

As a proof-of-concept, we demonstrated in the main text the algorithm and results specific to the spin-boson model. The method can be generalized to much more complicated systems. In the SI, we show the applicability of the HEOM+TTNS method for the Frenkel exciton model which is widely used in studying the excitation energy transfer in photosynthetic systems,⁴ as well as a spin-boson-like chain model where each spin is coupled to its own bosonic environment and the nearest-neighbor spins.

In summary, we presented the feasibility of adopting

a genuine TTNS and TDVP-based time propagation algorithm for solving the HEOM method, and compared its performance to the conventional HEOM method as well as the HEOM-MPS/TT scheme. Because the TTNS inherits many properties from the MPS/TT formalism, we expect that the proposed HEOM+TTNS method can also benefit from algorithmic optimizations and advances that have been developed in the context of the MPS/TT representation.^{81–87} Besides, we also hope that the idea presented in this work may inspire more applications of the tensor network states in combination with the HEOM method to enable a more efficient simulation of a much broader class of chemical and physical systems. For example, we will extend the current approach to study open fermionic system problems in our future work.^{88,89}

ACKNOWLEDGEMENTS

The author thanks M. Thoss for helpful discussions. This work was supported by the German Research Foundation (DFG).

SUPPLEMENTARY MATERIAL

See the supplementary material for the implementation details of the HEOM+TTNS method for the Frenkel exciton model and a spin-boson-like chain model.

DATA AVAILABILITY

The data and code that support the findings of this study are available from the corresponding author upon reasonable request.

- ¹H.-P. Breuer, F. Petruccione, *et al.*, *The theory of open quantum systems* (Oxford University Press on Demand, 2002).
- ²V. May and O. Kühn, *Charge and energy transfer dynamics in molecular systems* (John Wiley & Sons, 2008).
- ³H. Weimer, A. Kshetrimayum, and R. Orús, “Simulation methods for open quantum many-body systems,” *Rev. Mod. Phys.* **93**, 015008 (2021).
- ⁴A. Ishizaki and G. R. Fleming, “Theoretical examination of quantum coherence in a photosynthetic system at physiological temperature,” *Proceedings of the National Academy of Sciences* **106**, 17255–17260 (2009).
- ⁵J.-L. Brédas, E. H. Sargent, and G. D. Scholes, “Photovoltaic concepts inspired by coherence effects in photosynthetic systems,” *Nat. Mater.* **16**, 35–44 (2017).
- ⁶M. Thoss and F. Evers, “Perspective: Theory of quantum transport in molecular junctions,” *J. Chem. Phys.* **148**, 030901 (2018).
- ⁷J. C. Cuevas and E. Scheer, *Molecular electronics: an introduction to theory and experiment* (World Scientific, Singapore, 2010).
- ⁸Y. Tanimura and R. Kubo, “Time evolution of a quantum system in contact with a nearly gaussian-markoffian noise bath,” *J. Phys. Soc. Jpn.* **58**, 101–114 (1989).
- ⁹Y.-a. Yan, F. Yang, Y. Liu, and J. Shao, “Hierarchical approach based on stochastic decoupling to dissipative systems,” *Chem. Phys. Lett.* **395**, 216–221 (2004).

- ¹⁰R.-X. Xu and Y. Yan, “Dynamics of quantum dissipation systems interacting with bosonic canonical bath: Hierarchical equations of motion approach,” *Phys. Rev. E* **75**, 031107 (2007).
- ¹¹J. Jin, X. Zheng, and Y. Yan, “Exact dynamics of dissipative electronic systems and quantum transport: Hierarchical equations of motion approach,” *J. Chem. Phys.* **128**, 234703 (2008).
- ¹²Y. Yan, “Theory of open quantum systems with bath of electrons and phonons and spins: Many-dissipaton density matrixes approach,” *J. Chem. Phys.* **140**, 054105 (2014).
- ¹³C. Schinabeck, R. Härtle, and M. Thoss, “Hierarchical quantum master equation approach to electronic-vibrational coupling in nonequilibrium transport through nanosystems: Reservoir formulation and application to vibrational instabilities,” *Phys. Rev. B* **97**, 235429 (2018).
- ¹⁴C.-Y. Hsieh and J. Cao, “A unified stochastic formulation of dissipative quantum dynamics. i. generalized hierarchical equations,” *J. Chem. Phys.* **148**, 014103 (2018).
- ¹⁵L. Ye, X. Wang, D. Hou, R.-X. Xu, X. Zheng, and Y. Yan, “Heom-quick: a program for accurate, efficient, and universal characterization of strongly correlated quantum impurity systems,” *WIREs Comput Mol Sci* **6**, 608–638 (2016).
- ¹⁶Y. Tanimura, “Numerically “exact” approach to open quantum dynamics: The hierarchical equations of motion (heom),” *J. Chem. Phys.* **153**, 020901 (2020).
- ¹⁷A. Ishizaki and Y. Tanimura, “Quantum dynamics of system strongly coupled to low-temperature colored noise bath: Reduced hierarchy equations approach,” *J. Phys. Soc. Jpn.* **74**, 3131–3134 (2005).
- ¹⁸Q. Shi, L. Chen, G. Nan, R.-X. Xu, and Y. Yan, “Efficient hierarchical liouville space propagator to quantum dissipative dynamics,” *J. Chem. Phys.* **130**, 084105 (2009).
- ¹⁹J. Hu, R.-X. Xu, and Y. Yan, “Communication: Padé spectrum decomposition of fermi function and bose function,” *J. Chem. Phys.* **133**, 101106 (2010).
- ²⁰J. Strümpfer and K. Schulten, “Open quantum dynamics calculations with the hierarchy equations of motion on parallel computers,” *J. Chem. Theory Comput.* **8**, 2808–2816 (2012).
- ²¹M. Tsuchimoto and Y. Tanimura, “Spins dynamics in a dissipative environment: Hierarchical equations of motion approach using a graphics processing unit (gpu),” *J. Chem. Theory Comput.* **11**, 3859–3865 (2015).
- ²²T. Kramer, M. Noack, A. Reinefeld, M. Rodríguez, and Y. Zelinsky, “Efficient calculation of open quantum system dynamics and time-resolved spectroscopy with distributed memory heom (dm-heom),” *J. Comput. Chem.* **39**, 1779–1794 (2018).
- ²³Z.-H. Chen, Y. Wang, X. Zheng, R.-X. Xu, and Y. Yan, “Universal time-domain prony fitting decomposition for optimized hierarchical quantum master equations,” *J. Chem. Phys.* **156**, 221102 (2022).
- ²⁴M. Xu, Y. Yan, Q. Shi, J. Ankerhold, and J. Stockburger, “Taming quantum noise for efficient low temperature simulations of open quantum systems,” *Phys. Rev. Lett.* **129**, 230601 (2022).
- ²⁵T. Ikeda and A. Nakayama, “Collective bath coordinate mapping of “hierarchy” in hierarchical equations of motion,” *J. Chem. Phys.* **156**, 104104 (2022).
- ²⁶U. Schollwöck, “The density-matrix renormalization group in the age of matrix product states,” *Ann. Phys. (NY)* **326**, 96–192 (2011).
- ²⁷I. V. Oseledets, “Tensor-train decomposition,” *SIAM J. Sci. Comput.* **33**, 2295–2317 (2011).
- ²⁸Q. Shi, Y. Xu, Y. Yan, and M. Xu, “Efficient propagation of the hierarchical equations of motion using the matrix product state method,” *J. Chem. Phys.* **148**, 174102 (2018).
- ²⁹R. Borrelli, “Density matrix dynamics in twin-formulation: An efficient methodology based on tensor-train representation of reduced equations of motion,” *J. Chem. Phys.* **150**, 234102 (2019).
- ³⁰Y. Yan, T. Xing, and Q. Shi, “A new method to improve the numerical stability of the hierarchical equations of motion for discrete harmonic oscillator modes,” *J. Chem. Phys.* **153**, 204109 (2020).
- ³¹Y. Ke, R. Borrelli, and M. Thoss, “Hierarchical equations of motion approach to hybrid fermionic and bosonic environments: Matrix product state formulation in twin space,” *J. Chem. Phys.* **156**, 194102 (2022).
- ³²G. Vidal, “Efficient simulation of one-dimensional quantum many-body systems,” *Phys. Rev. Lett.* **93**, 040502 (2004).
- ³³Y.-Y. Shi, L.-M. Duan, and G. Vidal, “Classical simulation of quantum many-body systems with a tree tensor network,” *Phys. Rev. A* **74**, 022320 (2006).
- ³⁴L. Tagliacozzo, G. Evenbly, and G. Vidal, “Simulation of two-dimensional quantum systems using a tree tensor network that exploits the entropic area law,” *Phys. Rev. B* **80**, 235127 (2009).
- ³⁵V. Murg, F. Verstraete, Ö. Legeza, and R. M. Noack, “Simulating strongly correlated quantum systems with tree tensor networks,” *Phys. Rev. B* **82**, 205105 (2010).
- ³⁶W. Li, J. von Delft, and T. Xiang, “Efficient simulation of infinite tree tensor network states on the bethe lattice,” *Phys. Rev. B* **86**, 195137 (2012).
- ³⁷H. J. Changlani, S. Ghosh, C. L. Henley, and A. M. Läuchli, “Heisenberg antiferromagnet on cayley trees: Low-energy spectrum and even/odd site imbalance,” *Phys. Rev. B* **87**, 085107 (2013).
- ³⁸N. Nakatani and G. K.-L. Chan, “Efficient tree tensor network states (ttns) for quantum chemistry: Generalizations of the density matrix renormalization group algorithm,” *J. Chem. Phys.* **138**, 134113 (2013).
- ³⁹V. Murg, F. Verstraete, R. Schneider, P. R. Nagy, and O. Legeza, “Tree tensor network state with variable tensor order: An efficient multireference method for strongly correlated systems,” *J. Chem. Theory Comput.* **11**, 1027–1036 (2015).
- ⁴⁰K. Gunst, F. Verstraete, S. Wouters, O. Legeza, and D. Van Neck, “T3ns: Three-legged tree tensor network states,” *J. Chem. Theory Comput.* **14**, 2026–2033 (2018).
- ⁴¹F. A. Schröder, D. H. Turban, A. J. Musser, N. D. Hine, and A. W. Chin, “Tensor network simulation of multi-environmental open quantum dynamics via machine learning and entanglement renormalisation,” *Nat. Commun.* **10**, 1–10 (2019).
- ⁴²H. R. Larsson, “Computing vibrational eigenstates with tree tensor network states (ttns),” *J. Chem. Phys.* **151**, 204102 (2019).
- ⁴³G. Ferrari, G. Magnifico, and S. Montangero, “Adaptive-weighted tree tensor networks for disordered quantum many-body systems,” *Phys. Rev. B* **105**, 214201 (2022).
- ⁴⁴P. Seitz, I. Medina, E. Cruz, Q. Huang, and C. B. Mendl, “Simulating quantum circuits using tree tensor networks,” *arXiv preprint arXiv:2206.01000* (2022).
- ⁴⁵A. Milsted, M. Ganahl, S. Leichenauer, J. Hidary, and G. Vidal, “Tensornetwork on tensorflow: A spin chain application using tree tensor networks,” *arXiv preprint arXiv:1905.01331* (2019).
- ⁴⁶D. Bauernfeind and M. Aichhorn, “Time dependent variational principle for tree tensor networks,” *SciPost Physics* **8**, 024 (2020).
- ⁴⁷B. Kloss, D. Reichman, and Y. Bar Lev, “Studying dynamics in two-dimensional quantum lattices using tree tensor network states,” *SciPost Physics* **9**, 070 (2020).
- ⁴⁸G. Ceruti, C. Lubich, and H. Walach, “Time integration of tree tensor networks,” *SIAM J. Numer. Anal.* **59**, 289–313 (2021).
- ⁴⁹J. Hu, M. Luo, F. Jiang, R.-X. Xu, and Y. Yan, “Padé spectrum decompositions of quantum distribution functions and optimal hierarchical equations of motion construction for quantum open systems,” *J. Chem. Phys.* **134**, 244106 (2011).
- ⁵⁰T. Ikeda and G. D. Scholes, “Generalization of the hierarchical equations of motion theory for efficient calculations with arbitrary correlation functions,” *J. Chem. Phys.* **152**, 204101 (2020).
- ⁵¹M. Schmutz, “Real-time green’s functions in many body problems,” *Zeitschrift für Physik B Condensed Matter* **30**, 97–106 (1978).
- ⁵²M. Suzuki, “Density matrix formalism, double-space and thermo field dynamics in non-equilibrium dissipative systems,” *Internat. J. Modern Phys. B* **5**, 1821–1842 (1991).
- ⁵³T. Arimitsu and H. Umezawa, “Non-equilibrium thermo field dynamics,” *Prog. Theor. Phys.* **77**, 32–52 (1987).

- ⁵⁴A. E. Feiguin and S. R. White, “Finite-temperature density matrix renormalization using an enlarged hilbert space,” *Phys. Rev. B* **72**, 220401 (2005).
- ⁵⁵F. Verstraete, J. J. Garcia-Ripoll, and J. I. Cirac, “Matrix product density operators: Simulation of finite-temperature and dissipative systems,” *Phys. Rev. Lett.* **93**, 207204 (2004).
- ⁵⁶R. Borrelli and M. F. Gelin, “Finite temperature quantum dynamics of complex systems: Integrating thermo-field theories and tensor-train methods,” *WIREs Comput Mol Sci*, e1539 (2021).
- ⁵⁷L. Zhu, H. Liu, W. Xie, and Q. Shi, “Explicit system-bath correlation calculated using the hierarchical equations of motion method,” *J. Chem. Phys.* **137**, 194106 (2012).
- ⁵⁸L. Song and Q. Shi, “Hierarchical equations of motion method applied to nonequilibrium heat transport in model molecular junctions: Transient heat current and high-order moments of the current operator,” *Phys. Rev. B* **95**, 064308 (2017).
- ⁵⁹A. Kato and Y. Tanimura, “Quantum heat current under non-perturbative and non-markovian conditions: Applications to heat machines,” *J. Chem. Phys.* **145**, 224105 (2016).
- ⁶⁰J. I. Cirac and F. Verstraete, “Renormalization and tensor product states in spin chains and lattices,” *J. Phys. A Math. Theor.* **42**, 504004 (2009).
- ⁶¹G. K.-L. Chan, A. Keselman, N. Nakatani, Z. Li, and S. R. White, “Matrix product operators, matrix product states, and ab initio density matrix renormalization group algorithms,” *J. Chem. Phys.* **145**, 014102 (2016).
- ⁶²D. Jaschke, M. L. Wall, and L. D. Carr, “Open source matrix product states: Opening ways to simulate entangled many-body quantum systems in one dimension,” *Comput. Phys. Commun.* **225**, 59–91 (2018).
- ⁶³C. Lubich, T. Rohwedder, R. Schneider, and B. Vandereycken, “Dynamical approximation by hierarchical tucker and tensor-train tensors,” *SIAM J. Matrix Anal. Appl.* **34**, 470–494 (2013).
- ⁶⁴M. H. Beck and H.-D. Meyer, “An efficient and robust integration scheme for the equations of motion of the multiconfiguration time-dependent hartree (mctdh) method,” *Zeitschrift für Physik D Atoms, Molecules and Clusters* **42**, 113–129 (1997).
- ⁶⁵H. Wang and M. Thoss, “Multilayer formulation of the multiconfiguration time-dependent hartree theory,” *J. Chem. Phys.* **119**, 1289–1299 (2003).
- ⁶⁶H.-D. Meyer, F. Gatti, and G. A. Worth, *Multidimensional quantum dynamics: MCTDH theory and applications* (John Wiley & Sons, 2009).
- ⁶⁷U. Manthe, “The multi-configurational time-dependent hartree approach revisited,” *J. Chem. Phys.* **142**, 244109 (2015).
- ⁶⁸H. Wang, “Multilayer multiconfiguration time-dependent hartree theory,” *J. Phys. Chem. A* **119**, 7951–7965 (2015).
- ⁶⁹L. P. Lindoy, B. Kloss, and D. R. Reichman, “Time evolution of ml-mctdh wavefunctions. i. gauge conditions, basis functions, and singularities,” *J. Chem. Phys.* **155**, 174108 (2021).
- ⁷⁰S. Montangero, E. Rico, and P. Silvi, “Loop-free tensor networks for high-energy physics,” *Philos. Trans. R. Soc. A* **380**, 20210065 (2022).
- ⁷¹Y. Yan, M. Xu, T. Li, and Q. Shi, “Efficient propagation of the hierarchical equations of motion using the tucker and hierarchical tucker tensors,” *J. Chem. Phys.* **154**, 194104 (2021).
- ⁷²J. Haegeman, T. J. Osborne, and F. Verstraete, “Post-matrix product state methods: To tangent space and beyond,” *Phys. Rev. B* **88**, 075133 (2013).
- ⁷³C. Lubich, I. V. Oseledets, and B. Vandereycken, “Time integration of tensor trains,” *SIAM J. Numer. Anal.* **53**, 917–941 (2015).
- ⁷⁴J. Haegeman, C. Lubich, I. Oseledets, B. Vandereycken, and F. Verstraete, “Unifying time evolution and optimization with matrix product states,” *Phys. Rev. B* **94**, 165116 (2016).
- ⁷⁵F. A. Schröder and A. W. Chin, “Simulating open quantum dynamics with time-dependent variational matrix product states: Towards microscopic correlation of environment dynamics and reduced system evolution,” *Phys. Rev. B* **93**, 075105 (2016).
- ⁷⁶A. Baiardi and M. Reiher, “Large-scale quantum dynamics with matrix product states,” *J. Chem. Theory Comput.* **15**, 3481–3498 (2019).
- ⁷⁷C. B. Mendl, “Time evolution of matrix product operators with energy conservation,” arXiv preprint arXiv:1812.11876 (2018).
- ⁷⁸S. Paeckel, T. Köhler, A. Swoboda, S. R. Manmana, U. Schollwöck, and C. Hubig, “Time-evolution methods for matrix-product states,” *Ann. Phys. (NY)* **411**, 167998 (2019).
- ⁷⁹D. M. Wilkins and N. S. Dattani, “Why quantum coherence is not important in the fenna-matthews-olsen complex,” *J. Chem. Theory Comput.* **11**, 3411–3419 (2015).
- ⁸⁰M. Fishman, S. R. White, and E. M. Stoudenmire, “The ITensor Software Library for Tensor Network Calculations,” *SciPost Phys. Codebases*, 4 (2022).
- ⁸¹M. Yang and S. R. White, “Time-dependent variational principle with ancillary krylov subspace,” *Phys. Rev. B* **102**, 094315 (2020).
- ⁸²P. Secular, N. Gourianov, M. Lubasch, S. Dolgov, S. R. Clark, and D. Jaksch, “Parallel time-dependent variational principle algorithm for matrix product states,” *Phys. Rev. B* **101**, 235123 (2020).
- ⁸³A. J. Dunnett and A. W. Chin, “Efficient bond-adaptive approach for finite-temperature open quantum dynamics using the one-site time-dependent variational principle for matrix product states,” *Phys. Rev. B* **104**, 214302 (2021).
- ⁸⁴R. Borrelli and S. Dolgov, “Expanding the range of hierarchical equations of motion by tensor-train implementation,” *J. Phys. Chem. B* **125**, 5397–5407 (2021).
- ⁸⁵J.-W. Li, A. Gleis, and J. Von Delft, “Time-dependent variational principle with controlled bond expansion for matrix product states,” arXiv preprint arXiv:2208.10972 (2022).
- ⁸⁶Y. Xu, Z. Xie, X. Xie, U. Schollwöck, and H. Ma, “Stochastic adaptive single-site time-dependent variational principle,” *JACS Au* **2**, 335–340 (2022).
- ⁸⁷G. Ceruti, C. Lubich, and D. Sulz, “Rank-adaptive time integration of tree tensor networks,” *SIAM J. Numer. Anal.* **61**, 194–222 (2023).
- ⁸⁸Y. Ke, J. Dvořák, M. Čížek, R. Borrelli, and M. Thoss, “Current-induced bond rupture in single-molecule junctions: Effects of multiple electronic states and vibrational modes,” arXiv preprint arXiv:2304.09467 (2023).
- ⁸⁹P. Evers, A. Aharony, N. Bar-Gill, O. Entin-Wohlman, P. Hedegård, O. Hod, P. Jelinek, G. Kamieniarz, M. Lemesko, K. Michaeli, *et al.*, “Theory of chirality induced spin selectivity: Progress and challenges,” *Adv. Mater.* **34**, 2106629 (2022).